





Energy-chirp compensation of laser-driven ion beams enabled by structured targets

Zheng Gong ^{1,2,*}, Stepan S. Bulanov ³, Toma Toncian ⁴ and Alexey Arefiev ⁵

¹Center for High Energy Density Science, The University of Texas at Austin, Austin, Texas 78712, USA

²SKLNPT, KLHEDP, CAPT and School of Physics, Peking University, Beijing 100871, China

³Lawrence Berkeley National Laboratory, Berkeley, California 94720, USA

⁴Institute for Radiation Physics, Helmholtz-Zentrum Dresden-Rossendorf e.V., 01328 Dresden, Germany

⁵Department of Mechanical and Aerospace Engineering, University of California San Diego, La Jolla, California 92093, USA



(Received 4 May 2022; accepted 27 October 2022; published 21 November 2022)

We show using three-dimensional (3D) simulations that the challenge of generating dense monoenergetic laser-driven ion beams with low angular divergence can be overcome by utilizing structured targets with a relativistically transparent channel and an overdense wall. In contrast to a uniform target that produces a chirped ion beam, the target structure facilitates the formation of a dense electron bunch whose longitudinal electric field reverses the energy chirp. This approach works in conjunction with existing acceleration mechanisms, augmenting the ion spectra. For example, our 3D simulations predict a significant improvement for a 2 PW laser pulse with a peak intensity of 5×10^{22} W/cm². The simulations show a monoenergetic proton peak in a highly desirable energy range of 200 MeV with an unprecedented charge of several nC and a relatively low divergence that is below 10° .

DOI: [10.1103/PhysRevResearch.4.L042031](https://doi.org/10.1103/PhysRevResearch.4.L042031)

The development of laser-driven ion accelerators attracts considerable attention since the generated ion beams are essential to various cross-disciplinary applications [1–4]. State-of-the-art high-power laser systems [5–7] have the potential to enable compact and efficient high repetition rate ion accelerators. Depending on the interaction parameters, the ion acceleration can follow one of multiple scenarios [8]. The most studied and used scenario is target normal sheath acceleration (TNSA) [9–13], whereas the most efficient one in terms of energy transfer from the laser to the ions is radiation pressure acceleration (RPA) [14–18]. The successful realization of RPA requires ultrathin targets that stay intact during the interaction, but this can be hard to achieve due to laser prepulse and plasma instabilities [19–26]. These difficulties can be circumvented by employing acceleration mechanisms such as shockwave acceleration [27–29], hole-boring radiation pressure acceleration [30–32], and magnetic vortex acceleration (MVA) [33–40] that involve a thick plasma with a near-critical electron density, i.e., a density close to $n_{cr} \equiv m_e \omega^2 / 4\pi e^2 \approx 1.8 \times 10^{21}$ cm⁻³ for an 800-nm wavelength electromagnetic wave [1,41]. Here, ω is the carrier frequency of the laser pulse and m_e (e) is the electron mass (charge).

Most applications have requirements for individual particle energies and their collective charge [1–4]. Meeting both

requirements has proven to be extremely challenging for energies in excess of 100 MeV per nucleon. Achieving a required number of particles in a specific energy range is considered a grand challenge and a prerequisite for the wide utilization of high-power laser systems for a number of applications. For example, TNSA and MVA generate broad ion energy spectra that can contain very energetic ions [12]. However, the ion numbers decrease with energy, so there are very few of these ions, meaning that merely reaching high energies is insufficient for these mechanisms. Recent progress in target fabrication has opened up to experimental research novel target configurations [42–44] and reinvigorated the study of laser-driven ion acceleration. These configurations have the potential to relax what was previously perceived as fundamental constraints, e.g., the inability to produce monoenergetic peaks for certain otherwise promising acceleration mechanisms such as MVA.

In this Letter, we show using three-dimensional (3D) kinetic particle-in-cell (PIC) simulations how a proton acceleration mechanism that generates a broad spectrum with a monotonically decreasing number of energetic particles can be augmented to achieve a monoenergetic peak. A nontrivial physics phenomenon is the emergence of a dense forward-moving electron bunch enabled by a structured target with a prefilled channel as shown in Fig. 1(a) and a strong plasma magnetic field. Prior to the arrival of the bunch, the ions have a positive chirp with the ion energy increasing along the axis. The bunch generates a strong positive longitudinal electric field, so, as it catches up with the energetic ions, this field compensates the chirp by accelerating the lower-energy ions and produces a monoenergetic peak in the ion spectrum. The electron bunch has also a focusing transverse electric field that reduces the divergence of the accelerated protons. We refer to the described mechanism as laser ion-shotgun

*Present address: Max-Planck-Institut für Kernphysik, Saupfercheckweg 1, 69117 Heidelberg, Germany.

Published by the American Physical Society under the terms of the Creative Commons Attribution 4.0 International license. Further distribution of this work must maintain attribution to the author(s) and the published article's title, journal citation, and DOI.

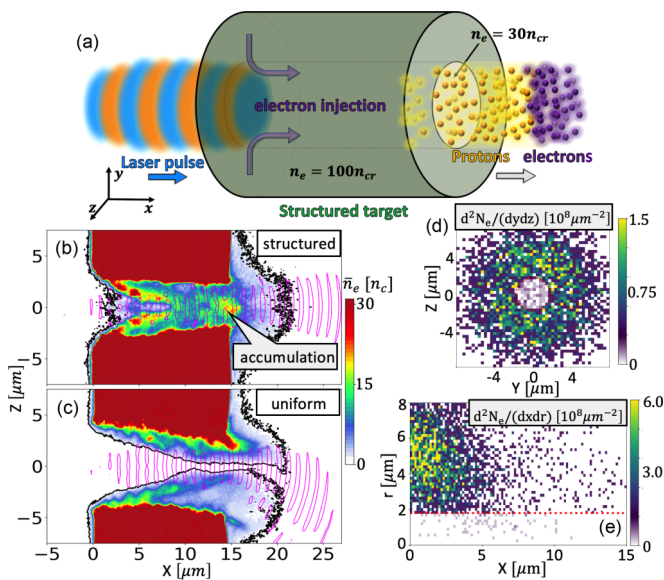


FIG. 1. (a) Schematic setup. (b) and (c) Time-averaged electron densities \bar{n}_e in the (x, z) plane at $y = 0$ for structured and uniform targets. Black and magenta contours correspond to $\bar{n}_e = n_{cr}$ and $a_0 = 60$. (d) and (e) Initial location of the electrons from the bunch located in (b) at $12 \mu\text{m} < x < 16 \mu\text{m}$, $r < 2 \mu\text{m}$, and marked as “accumulation.” The dotted red line is the initial location of the channel wall.

acceleration (LISA), because the channel is akin to a barrel of a shotgun that builds up an expulsion force and propels a bullet—the collimated proton beam in our case. We note that the structured targets, which enable LISA, have evolved from being a concept [45] to a commercial product used in experiments [44] in the period of just 6 years.

Structured versus uniform target. We have performed two 3D PIC simulations using the fully relativistic code EPOCH [46]: a simulation with the structured target from Fig. 1(a) and a simulation with a uniform target with density equal to the density of the channel. Both simulations use the same linearly polarized 2-PW laser ($\lambda_0 = 1 \mu\text{m}$ wavelength) focused at the target surface ($x = 0$). In the absence of the target, the transverse laser electric field in the focal plane is $E_y = E_0 \exp(-r^2/w_0^2) \exp[-4(ct - x)^2/(c\tau)^2] \cos(\omega t)$, where $w_0 = 2.2 \mu\text{m}$ and $\tau = 120$ fs. The normalized laser amplitude $a_0 \equiv |e|E_0/m_e c \omega \approx 190$ corresponds to a peak laser intensity of $5 \times 10^{22} \text{ W/cm}^2$, where c is the speed of light. The uniform target is a hydrogenic plasma with electron density $n_e = 30n_{cr}$. The structured target has a cylindrical channel of radius $R_{ch} = 1.8 \mu\text{m}$ that is filled with the same plasma. The bulk is a carbon plasma with $n_e = 100n_{cr}$. Both targets are $L_T = 15 \mu\text{m}$ thick. We use 50 (10) macroparticles per cell to represent ions (electrons). The simulation domain is $60 \mu\text{m} \times 30 \mu\text{m} \times 30 \mu\text{m}$ with $1200 \times 360 \times 360$ cells.

As the high-intensity laser starts to interact with these targets, it quickly ionizes them. Then the laser is guided through these targets, where either a self-generated channel [Fig. 1(c)] or the premanufactured channel [Fig. 1(b)] facilitate this. Since the thickness of these targets is rather small, they are transparent to the relativistically intense laser pulses, i.e., the thickness is smaller than the depletion length of the laser

pulse in the plasma of such density [35,36,40], $L_T < L_D = (c\tau K)(a_{ch}n_{cr})/n_e$, which is around $40 \mu\text{m}$ for the given laser and plasma parameters. Here, $K = 0.074$ is the geometrical factor from the depletion length calculation [35,36,40] and a_{ch} is the field amplitude inside the plasma channel. As the laser pulse exits the target, a proton acceleration regime similar to the MVA takes place in both cases, with a cutoff energy of about 450 MeV

However, there are important distinctions between these two targets. First, a structured target provides a more stable propagation of an intense laser pulse due to high-density walls [compare Figs. 1(b) and 1(c)]. Second, during the interaction a forward-moving electron density maximum is formed near the exit of the channel [see Fig. 1(b)], which is absent in the other case. Such an electron density evolution leads to the formation of strong forward-moving focusing and accelerating for proton electric fields. This results in a sharp peak in the proton spectrum around 220 MeV [see Fig. 2(c)]. This is exactly the MVA spectrum augmentation, which was mentioned above.

In what follows we describe in detail the laser pulse interaction with a structured target and discuss the underlying physical mechanisms, which generate a high-charge, well-collimated proton bunch.

Electron extraction. When the laser transverse electric field E_y is imposed on the front surface of the target bulk, the electrons originating from the bulk inner edge are prone to be extracted by the field E_y . Then, these injected electrons with an imprinted transverse momentum $p_y \sim |e|E_y/(m_e c \omega)$ are deflected by the magnetic force $(\mathbf{p}_y/\gamma) \times \mathbf{B}$ to move forward. The density of these electrons can be estimated from requiring the balance between the energy gain in the ponderomotive potential and in the field of the ion core in the channel [35,36,40]. Then, we obtain

$$n_e/n_{cr} = (2/K)^{1/2} (\lambda/\pi R_{ch})^3 (P/P_c)^{1/2}, \quad (1)$$

where P is the laser power and $P_c = 2m_e^2 c^5 / e^2 = 17 \text{ GW}$. Then, the magnetic field, generated by these electrons, is of the order of $eB/m\omega c = rn_e/\lambda n_{cr}$ for $r < R_{ch}$, or from Eq. (1),

$$eB/m\omega c = (2/K)^{1/2} (r\lambda^2/\pi^3 R_{ch}^3) (P/P_c)^{1/2}. \quad (2)$$

The maximum value of this field at $r = R_{ch}$ is

$$B_{\max} = 0.12 E_0 \lambda / R_{ch}, \quad (3)$$

where E_0 is the laser peak field. In Figs. 1(d) and 1(e), the distribution of the initial position of electrons [marked by “accumulation” in Fig. 1(b)] demonstrates that electrons, which maintain a strong electric field, come from the front side of the target bulk region. Therefore, the merits of channel structure are not only guiding the light propagation but also providing a sufficient electron population to generate a strong longitudinal electric field for proton acceleration [see Fig. 2(a)].

Energy-chirp compensation. The distribution of protons within the divergence angle $\theta = \arctan(p_r/p_x) < 10^\circ$ in (x, p_x) space is shown in Fig. 2(b), where $p_r = (p_y^2 + p_z^2)^{1/2}$. The field E_x actively piles up a dense bunch proton with the momentum $p_x \sim 0.7m_p c$ and kinetic energy $\varepsilon_p \sim 200 \text{ MeV}$ at $t = 340$ fs. After interaction with the moving E_x , this piled-up proton bunch has a monoenergetic feature in the energy spectrum, shown as the red solid line in Fig. 2(c), where the spectrum (red dotted line) before the interaction at $t = 240$ fs

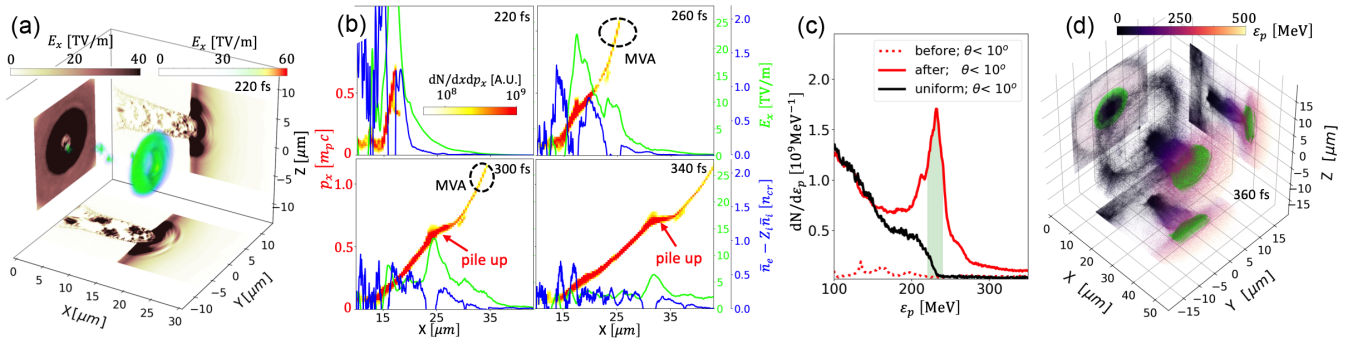


FIG. 2. (a) Longitudinal electric field E_x where the projections exhibit the distribution at the slice of $x = 16 \mu\text{m}$, $y = 0$, and $z = 0$. (b) Proton distribution in x - p_x space, where the green line profiles the field E_x and the blue line denotes the net charge density $\bar{n}_e - Z_i \bar{n}_i$. (c) Proton energy spectra. (d) The distribution of the generated proton beams, where the lime dots represent the protons within energy range of $220 < \varepsilon_p [\text{MeV}] < 240$ [shadow green area in (d)].

is also plotted for comparison. Here, the proton energy spectrum of the case with the same parameters but a uniform target is profiled as well to certify that the monoenergetic proton bunch is a unique feature for the acceleration mechanism involved with the structured channel target. The spatial distribution of the protons in Fig. 2(d) indicates that an energetic dense proton beam is produced, where the lime dots represent the protons within the energy range of 220–240 MeV [shadow green area in Fig. 2(c)].

For figuring out how the proton bunch is spontaneously piled up by the moving field E_x , we perform a detailed particle tracking of the protons near the peak energy of the spectrum [shadow green area in Fig. 2(c)]. The proton distribution in x - p_x space for a time from $t = 200$ to 360 fs [see Fig. 3(a)] indicates that the proton bunch with a negative energy chirp $[-\partial \mathcal{E}_p(x)/\partial x < 0]$ experiences a longitudinally descending accelerating field $[\partial E_x(x)/\partial x < 0]$. The stronger E_x is imposed on the protons with a lower energy, which results in the elimination of the proton energy chirp. Specifically, the relative energy spread is reduced from almost 100% to 8.7% at the end of the chirp compensation process. In order to understand the dynamics of protons, we approximate the amplitude of the moving field as $E_x(x) = (40\tau/T_0)(m_e c \omega / |e|) / \{(x/\lambda_0 - 8)^2 + \tau/T_0\}$, by fitting the evolution of the field that protons experience from PIC simulation results. Here, T_0 is the period of the electromagnetic (EM) field of the laser. This approximation proves to be rather accurate as it can be seen from Fig. 3(b), where the evolutions of the proton bunch phase space obtained

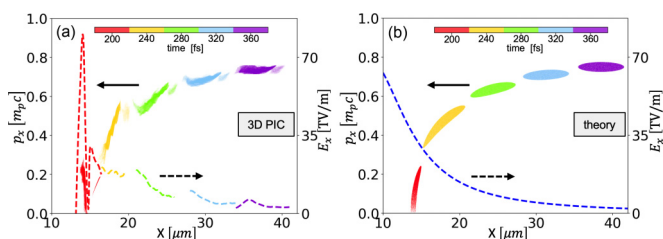


FIG. 3. (a) Proton distribution in (x, p_x) space, where the colors correspond to different times and dashed lines denote the field E_x imposed on the proton bunch. (b) is the same as (a) but for the theoretically predicted proton evolution, where the blue dashed line refers to the estimated electric field.

from the PIC simulation and from the approximation are shown.

Transverse focusing. After the laser reaches the rear side and exits the target, the quasistatic transverse electric field [Fig. 4(a)] induced by the forward electron flow acts as a focusing lens collimating the accelerated protons. The outward proton momentum (p_y and p_z) is gradually counteracted by the focusing electric fields \bar{E}_y and \bar{E}_z [Fig. 4(b)], where the bar denotes time averaging over two laser periods. The inward radial electric field \bar{E}_r [Fig. 4(c)] is ~ 10 TV/m, so it reduces the proton divergence angle by 15° within 100 fs. We approximate the radial electric field acting on the protons by $\bar{E}_r = -\kappa_1 r \hat{e}_r$, where $\kappa_1 > 0$ is a constant. The transverse proton motion in this field evolves according to the equation

$$\frac{d^2 r}{dt^2} + \frac{|e| \kappa_1}{m_p \gamma} r + \frac{p_r}{m_p \gamma^2} \frac{d\gamma}{dt} = 0, \quad (4)$$

obtained by combining $dr/dt = p_r/(\gamma m_p)$ and $dp_r/dt = -|e| \kappa_1 r$. On account of $\gamma \sim 1$ and the third term on the left-hand side of Eq. (4) being negligible compared to the second term, the solution of Eq. (4) reads $[r(t), p_r(t)]^T = \mathcal{M}_f [r(t-t_0), p_r(t-t_0)]^T$. The focusing effect of the field E_r on protons is incorporated into the transmission matrix

$$\mathcal{M}_f = \begin{Bmatrix} \cos[\Omega_k(t-t_0)] & \frac{1}{\Omega_k} \sin[\Omega_k(t-t_0)] \\ -\Omega_k \sin[\Omega_k(t-t_0)] & \cos[\Omega_k(t-t_0)] \end{Bmatrix}, \quad (5)$$

where $\Omega_k = \sqrt{|e| \kappa_1 / m_p \gamma}$ and t_0 is the initial time.

In the focusing field, the protons with large divergence $\theta \sim 30^\circ$ are gradually collimated to a cone of $\theta \sim 10^\circ$ [lower panel of Fig. 4(d)]. If a bunch of protons is initialized within an ellipse in (r, θ) space, the theoretically predicted proton evolution [upper panel of Fig. 4(d)] based on the transmission matrix \mathcal{M}_f with $\kappa_1 = 3.6\pi m_e c^2 / (|e| \lambda^2) \approx 5.8 \times 10^{18} \text{ V/m}^2$ in Eq. (5) is in reasonable agreement with the PIC simulation results. The collimation effect can also be seen by comparing the proton distribution in the transverse momentum plane (p_y, p_z) prior to (or after) the arrival of the forward-moving electron population [Fig. 4(e)]. After the transverse focusing, a strong pinching effect leads to the proton concentrating in a cone of $\theta < 10^\circ$, whereas the distribution has a ring-type structure that is rather broad, with a characteristic opening angle of $\theta \approx 20^\circ$ before the focusing.

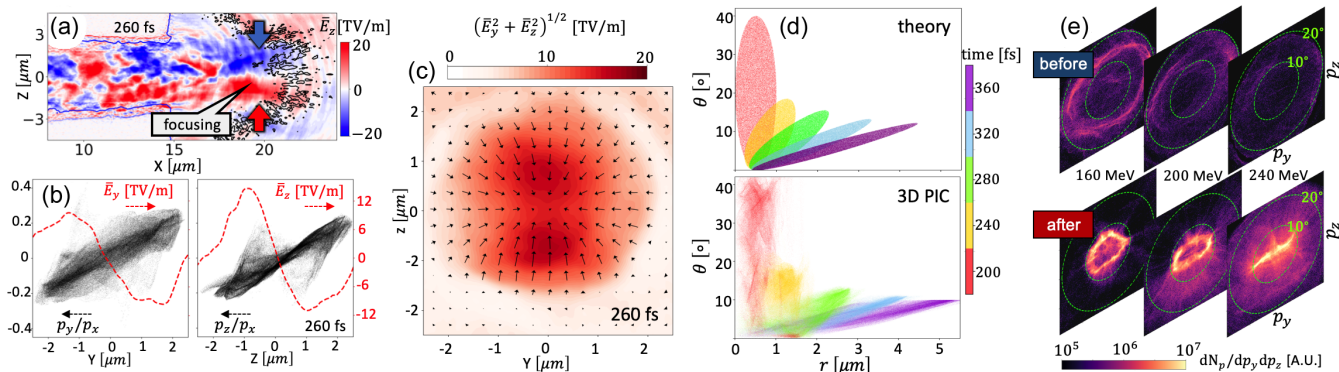


FIG. 4. (a) Transverse electric field \bar{E}_z at the slice of $y = 0$. (b) Distribution of protons in transverse p_y - y (p_z - z) space. (c) Radial focusing electric field $\bar{E}_r = (\bar{E}_y^2 + \bar{E}_z^2)^{1/2}$ averaged over $18 < x [\mu\text{m}] < 21$ where black arrows denote the field direction. (d) Time evolution of the protons within the monoenergetic part $220 < \epsilon_p [\text{MeV}] < 240$ in r - θ space. (e) Proton angular distribution *before* and *after* the transversely focusing process.

Discussion. The presented mechanism has two distinct stages. The proton energy gain primarily happens during the initial stage that is present for both uniform and structured targets and is characterized by a broad proton spectrum with a sharp cutoff. The energy-chirp compensation and focusing occur during the second stage that is only present when using structured targets.

We have performed four scans, shown in Fig. 5, to establish the dependence of the monoenergetic peak’s energy ϵ_p^{peak} on the target and laser parameters. Each marker represents a separate 3D PIC simulation. In each scan, only a single parameter is varied while the other parameters remain the same as in the original simulation presented earlier. We find that ϵ_p^{peak} increases with both the normalized laser amplitude a_0 and with the laser pulse duration τ . The increase with τ is particularly noteworthy, because it indicates there is an advantage of using such longer laser pulses as the 150-fs pulse of the L4 laser at ELI Beamlines [5]. The scans over the channel, $n_{e,\text{in}}$, and bulk, $n_{e,\text{out}}$, densities shows that ϵ_p^{peak} is not particularly sensitive to these parameters over the explored range. In this Letter, we have deliberately explored the channel densities feasible for commercially available targets [44]. Even though the channel

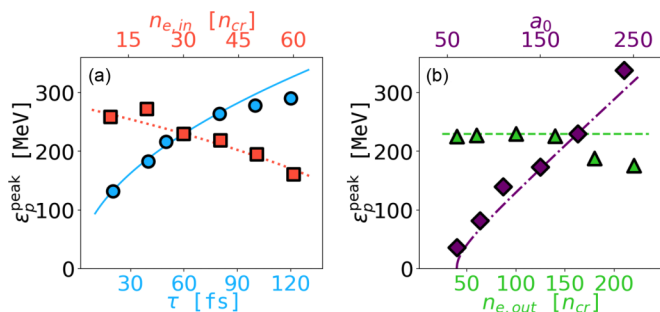


FIG. 5. Estimates (curves: blue solid, red dotted, green dashed, purple dotted-dashed) for peak energies ϵ_p^{peak} together with 3D PIC results (circles, squares, triangles, and diamonds) are shown for different values of (a) laser pulse duration τ and channel plasma density $n_{e,\text{in}}$, and (b) wall density $n_{e,\text{out}}$ and normalized laser field amplitude a_0 . The range of a_0 corresponds to a range of laser power from 0.15 to 3.5 PW.

densities are well controlled, the observed lack of sensitivity is an important safeguard against possible fluctuations that can occur during target fabrication. Finally, it is important to mention that the proton charge associated with the monoenergetic peak (defined by the condition $|\epsilon_p - \epsilon_p^{\text{peak}}| < 20 \text{ MeV}$) remains relatively high in all four scans, varying between 1 and 12 nC.

Summary and conclusions. We have presented a mechanism of laser-driven ion acceleration that can generate a monoenergetic proton peak in a highly desirable energy range of 200 MeV with an unprecedented charge of several nC and a relatively low divergence that is below 10° . The mechanism is enabled by a target design that has been recently employed in experiments with high-power, high-intensity lasers [44]. The laser power and intensity used in our study are either within reach or are already available at multi-PW laser facilities such as ELI-NP, CoReLS, and ZEUS [5,47]. Due to the combination of these factors, this work is an essential step towards solving the critical problem of generating high-charge proton beams with energies in excess of 100 MeV.

Our approach also opens up another avenue, associated with structured targets, within an established area of laser-driven ion acceleration. The use of these targets can potentially relax the requirements on the laser contrast and allow high repetition rate operations. The latter can be enabled by the use of a tape drive similar to the one discussed in Ref. [48].

The prefilled channel is essential for the stabilization of laser propagation and for the generation of strong transverse and longitudinal drift electric fields by pinched laser-accelerated electrons. As the field moves with the pinched electron current through an expanding energetic proton cloud at the back of the target, it focuses protons into a well-defined collimated quasimonoenergetic beam. We present an example, where a 2-PW, 120-fs laser can produce a quasimonoenergetic peak centered at 230 MeV via our mechanism. The number of protons in a 40 MeV energy interval is about 5×10^{10} particles, which is equivalent to a charge of 7.8 nC. These parameters are relevant to various applications that require high-energy, high repetition rate, high-charge, quasimonoenergetic proton sources.

Note added. Recently, we became aware of Refs. [49,50], where ion acceleration from laser-irradiated channel targets was investigated as well. These studies provide optimized parameters for improving the ion beam quality.

Acknowledgments. This research was supported under the National Science Foundation–Czech Science Foundation partnership by NSF Award No. PHY-2206777 and by AFOSR (Contract No. FA9550-17-1-0382). S.S.B. ac-

knowledges support from the U.S. Department of Energy Office of Science Offices of High Energy Physics and Fusion Energy Sciences (through LaserNetUS), under Contract No. DE-AC02-05CH11231. Simulations were performed using EPOCH [46], developed under U.K. EPSRC Grants No. EP/G054940, No. EP/G055165, and No. EP/G056803. High-performance computing (HPC) resources were provided by TACC.

-
- [1] G. A. Mourou, T. Tajima, and S. V. Bulanov, Optics in the relativistic regime, *Rev. Mod. Phys.* **78**, 309 (2006).
- [2] H. Daido, M. Nishiuchi, and A. S. Pirozhkov, Review of laser-driven ion sources and their applications, *Rep. Prog. Phys.* **75**, 056401 (2012).
- [3] A. Macchi, M. Borghesi, and M. Passoni, Ion acceleration by superintense laser-plasma interaction, *Rev. Mod. Phys.* **85**, 751 (2013).
- [4] S. V. Bulanov, J. J. Wilkens, T. Z. Esirkepov, G. Korn, G. Kraft, S. D. Kraft, M. Molls, and V. S. Khoroshkov, Laser ion acceleration for hadron therapy, *Phys. Usp.* **57**, 1149 (2014).
- [5] C. N. Danson, C. Haefner, J. Bromage, T. Butcher, J.-C. F. Chanteloup, E. A. Chowdhury, A. Galvanauskas, L. A. Gizzi, J. Hein, D. I. Hillier *et al.*, Petawatt and exawatt class lasers worldwide, *High Power Laser Sci. Eng.* **7**, e54 (2019).
- [6] K. Tanaka, K. Spohr, D. Balabanski, S. Balascuta, L. Capponi, M. Cernaianu, M. Cuciuc, A. Cucoanes, I. Dancus, A. Dhal *et al.*, Current status and highlights of the ELI-NP research program, *Matter Radiat. Extremes* **5**, 024402 (2020).
- [7] J. W. Yoon, Y. G. Kim, I. W. Choi, J. H. Sung, H. W. Lee, S. K. Lee, and C. H. Nam, Realization of laser intensity over 10^{23} W/cm², *Optica* **8**, 630 (2021).
- [8] S. S. Bulanov, E. Esarey, C. B. Schroeder, S. V. Bulanov, T. Z. Esirkepov, M. Kando, F. Pegoraro, and W. P. Leemans, Radiation pressure acceleration: The factors limiting maximum attainable ion energy, *Phys. Plasmas* **23**, 056703 (2016).
- [9] S. C. Wilks, A. B. Langdon, T. E. Cowan, M. Roth, M. Singh, S. Hatchett, M. H. Key, D. Pennington, A. MacKinnon, and R. A. Snavely, Energetic proton generation in ultra-intense laser-solid interactions, *Phys. Plasmas* **8**, 542 (2001).
- [10] P. Mora, Plasma Expansion into a Vacuum, *Phys. Rev. Lett.* **90**, 185002 (2003).
- [11] M. Roth and M. Schollmeier, Ion acceleration: TNSA, in *Laser-Plasma Interactions and Applications*, edited by D. Neely, D. Jaroszynski, P. McKenna, and R. Bingham (Springer, Cham, 2013), p. 303.
- [12] F. Wagner, O. Deppert, C. Brabetz, P. Fiala, A. Kleinschmidt, P. Poth, V. Schanz, A. Tebartz, B. Zielbauer, M. Roth, T. Stöhlker, and V. Bagnoud, Maximum Proton Energy above 85 MeV from the Relativistic Interaction of Laser Pulses with Micrometer Thick CH₂ Targets, *Phys. Rev. Lett.* **116**, 205002 (2016).
- [13] X. F. Shen, A. Pukhov, and B. Qiao, Monoenergetic High-Energy Ion Source via Femtosecond Laser Interacting with a Microtape, *Phys. Rev. X* **11**, 041002 (2021).
- [14] T. Esirkepov, M. Borghesi, S. V. Bulanov, G. Mourou, and T. Tajima, Highly Efficient Relativistic-Ion Generation in the Laser-Piston Regime, *Phys. Rev. Lett.* **92**, 175003 (2004).
- [15] X. Q. Yan, C. Lin, Z. M. Sheng, Z. Y. Guo, B. C. Liu, Y. R. Lu, J. X. Fang, and J. E. Chen, Generating High-Current Monoenergetic Proton Beams by a Circularly Polarized Laser Pulse in the Phase-Stable Acceleration Regime, *Phys. Rev. Lett.* **100**, 135003 (2008).
- [16] A. Macchi, S. Veghini, and F. Pegoraro, “Light Sail” Acceleration Reexamined, *Phys. Rev. Lett.* **103**, 085003 (2009).
- [17] B. Qiao, M. Zepf, M. Borghesi, and M. Geissler, Stable GeV Ion-Beam Acceleration from Thin Foils by Circularly Polarized Laser Pulses, *Phys. Rev. Lett.* **102**, 145002 (2009).
- [18] I. J. Kim, K. H. Pae, I. W. Choi, C.-L. Lee, H. T. Kim, H. Singhal, J. H. Sung, S. K. Lee, H. W. Lee, P. V. Nickles *et al.*, Radiation pressure acceleration of protons to 93 MeV with circularly polarized petawatt laser pulses, *Phys. Plasmas* **23**, 070701 (2016).
- [19] M. Kaluza, J. Schreiber, M. I. K. Santala, G. D. Tsakiris, K. Eidmann, J. Meyer-ter-Vehn, and K. J. Witte, Influence of the Laser Prepulse on Proton Acceleration in Thin-Foil Experiments, *Phys. Rev. Lett.* **93**, 045003 (2004).
- [20] P. McKenna, D. Carroll, O. Lundh, F. Nürnberg, K. Markey, S. Bandyopadhyay, D. Batani, R. Evans, R. Jafer, S. Kar *et al.*, Effects of front surface plasma expansion on proton acceleration in ultraintense laser irradiation of foil targets, *Laser Part. Beams* **26**, 591 (2008).
- [21] S. Steinke, A. Henig, M. Schnürer, T. Sokollik, P. Nickles, D. Jung, D. Kiefer, R. Hörlein, J. Schreiber, T. Tajima *et al.*, Efficient ion acceleration by collective laser-driven electron dynamics with ultra-thin foil targets, *Laser Part. Beams* **28**, 215 (2010).
- [22] F. Pegoraro and S. V. Bulanov, Photon Bubbles and Ion Acceleration in a Plasma Dominated by the Radiation Pressure of an Electromagnetic Pulse, *Phys. Rev. Lett.* **99**, 065002 (2007).
- [23] F. Dollar, C. Zwick, A. G. R. Thomas, V. Chvykov, J. Davis, G. Kalinchenko, T. Matsuoka, C. McGuffey, G. M. Petrov, L. Willingale, V. Yanovsky, A. Maksimchuk, and K. Krushelnick, Finite Spot Effects on Radiation Pressure Acceleration from Intense High-Contrast Laser Interactions with Thin Targets, *Phys. Rev. Lett.* **108**, 175005 (2012).
- [24] A. Sgattoni, S. Sinigardi, L. Fedeli, F. Pegoraro, and A. Macchi, Laser-driven Rayleigh-Taylor instability: Plasmonic effects and three-dimensional structures, *Phys. Rev. E* **91**, 013106 (2015).
- [25] Y. Wan, C.-H. Pai, C. J. Zhang, F. Li, Y. P. Wu, J. F. Hua, W. Lu, Y. Q. Gu, L. O. Silva, C. Joshi, and W. B. Mori, Physical Mechanism of the Transverse Instability in Radiation Pressure Ion Acceleration, *Phys. Rev. Lett.* **117**, 234801 (2016).
- [26] Y. Wan, I. A. Andriyash, W. Lu, W. B. Mori, and V. Malka, Effects of the Transverse Instability and Wave Breaking on

- the Laser-Driven Thin Foil Acceleration, *Phys. Rev. Lett.* **125**, 104801 (2020).
- [27] L. O. Silva, M. Marti, J. R. Davies, R. A. Fonseca, C. Ren, F. S. Tsung, and W. B. Mori, Proton Shock Acceleration in Laser-Plasma Interactions, *Phys. Rev. Lett.* **92**, 015002 (2004).
- [28] D. Haberberger, S. Tochitsky, F. Fiuza, C. Gong, R. A. Fonseca, L. O. Silva, W. B. Mori, and C. Joshi, Collisionless shocks in laser-produced plasma generate monoenergetic high-energy proton beams, *Nat. Phys.* **8**, 95 (2012).
- [29] H. Zhang, B. F. Shen, W. P. Wang, S. H. Zhai, S. S. Li, X. M. Lu, J. F. Li, R. J. Xu, X. L. Wang, X. Y. Liang, Y. X. Leng, R. X. Li, and Z. Z. Xu, Collisionless Shock Acceleration of High-Flux Quasimonoenergetic Proton Beams Driven by Circularly Polarized Laser Pulses, *Phys. Rev. Lett.* **119**, 164801 (2017).
- [30] Y. Sentoku, T. Cowan, A. Kemp, and H. Ruhl, High energy proton acceleration in interaction of short laser pulse with dense plasma target, *Phys. Plasmas* **10**, 2009 (2003).
- [31] A. Robinson, P. Gibbon, M. Zepf, S. Kar, R. Evans, and C. Bellei, Relativistically correct hole-boring and ion acceleration by circularly polarized laser pulses, *Plasma Phys. Controlled Fusion* **51**, 024004 (2009).
- [32] N. Naumova, T. Schlegel, V. T. Tikhonchuk, C. Labaune, I. V. Sokolov, and G. Mourou, Hole Boring in a DT Pellet and Fast-Ion Ignition with Ultraintense Laser Pulses, *Phys. Rev. Lett.* **102**, 025002 (2009).
- [33] A. V. Kuznetsov, T. Z. Esirkepov, F. F. Kamenets, and S. V. Bulanov, Efficiency of ion acceleration by a relativistically strong laser pulse in an underdense plasma, *Plasma Phys. Rep.* **27**, 211 (2001).
- [34] Y. Fukuda, A. Ya. Faenov, M. Tampo, T. A. Pikuz, T. Nakamura, M. Kando, Y. Hayashi, A. Yogo, H. Sakaki, T. Kameshima *et al.*, Energy Increase in Multi-MeV Ion Acceleration in the Interaction of a Short Pulse Laser with a Cluster-Gas Target, *Phys. Rev. Lett.* **103**, 165002 (2009).
- [35] S. S. Bulanov, V. Y. Bychenkov, V. Chvykov, G. Kalinchenko, D. W. Litzenberg, T. Matsuoka, A. G. R. Thomas, L. Willingale, V. Yanovsky, K. Krushelnick, and A. Maksimchuk, Generation of GeV protons from 1 PW laser interaction with near critical density targets, *Phys. Plasmas* **17**, 043105 (2010).
- [36] S. S. Bulanov, E. Esarey, C. B. Schroeder, W. P. Leemans, S. V. Bulanov, D. Margarone, G. Korn, and T. Haberer, Helium-3 and helium-4 acceleration by high power laser pulses for hadron therapy, *Phys. Rev. ST Accel. Beams* **18**, 061302 (2015).
- [37] T. Nakamura, S. V. Bulanov, T. Z. Esirkepov, and M. Kando, High-Energy Ions from Near-Critical Density Plasmas via Magnetic Vortex Acceleration, *Phys. Rev. Lett.* **105**, 135002 (2010).
- [38] M. H. Helle, D. F. Gordon, D. Kaganovich, Y. Chen, J. P. Palastro, and A. Ting, Laser-Accelerated Ions from a Shock-Compressed Gas Foil, *Phys. Rev. Lett.* **117**, 165001 (2016).
- [39] A. Sharma, High Energy electron and proton acceleration by circularly polarized laser pulse from near critical density hydrogen gas target, *Sci. Rep.* **8**, 2191 (2018).
- [40] J. Park, S. S. Bulanov, J. Bin, Q. Ji, S. Steinke, J.-L. Vay, C. G. R. Geddes, C. B. Schroeder, W. P. Leemans, T. Schenkel, and E. Esarey, Ion acceleration in laser generated megatesla magnetic vortex, *Phys. Plasmas* **26**, 103108 (2019).
- [41] E. Esarey, C. B. Schroeder, and W. P. Leemans, Physics of laser-driven plasma-based electron accelerators, *Rev. Mod. Phys.* **81**, 1229 (2009).
- [42] J. Snyder, L. L. Ji, K. M. George, C. Willis, G. E. Cochran, R. L. Daskalova, A. Handler, T. Rubin, P. L. Poole, D. Nasir, A. Zingale, E. Chowdhury, B. F. Shen, and D. W. Schumacher, Relativistic laser driven electron accelerator using micro-channel plasma targets, *Phys. Plasmas* **26**, 033110 (2019).
- [43] M. Bailly-Grandvaux, D. Kawahito, C. McGuffey, J. Strehlow, B. Edghill, M. S. Wei, N. Alexander, A. Haid, C. Brabetz, V. Bagnoud, R. Hollinger, M. G. Capeluto, J. J. Rocca, and F. N. Beg, Ion acceleration from microstructured targets irradiated by high-intensity picosecond laser pulses, *Phys. Rev. E* **102**, 021201(R) (2020).
- [44] H. Rinderknecht, T. Wang, A. L. Garcia, G. Bruhaug, M. Wei, H. Quevedo, T. Ditmire, J. Williams, A. Haid, D. Doria *et al.*, Relativistically transparent magnetic filaments: Scaling laws, initial results and prospects for strong-field QED studies, *New J. Phys.* **23**, 095009 (2021).
- [45] D. J. Stark, T. Toncian, and A. V. Arefiev, Enhanced Multi-MeV Photon Emission by a Laser-Driven Electron Beam in a Self-Generated Magnetic Field, *Phys. Rev. Lett.* **116**, 185003 (2016).
- [46] T. Arber, K. Bennett, C. Brady, A. Lawrence-Douglas, M. Ramsay, N. Sircombe, P. Gillies, R. Evans, H. Schmitz, A. Bell *et al.*, Contemporary particle-in-cell approach to laser-plasma modelling, *Plasma Phys. Controlled Fusion* **57**, 113001 (2015).
- [47] J. Nees, A. Maksimchuk, G. Kalinchenko, B. Hou, Y. Ma, P. Campbell, A. McKelvey, L. Willingale, I. Jovanovic, C. Kuranz, A. Thomas, and K. Krushelnick, ZEUS: A National Science Foundation mid-scale facility for laser-driven science in the QED regime, in *Conference on Lasers and Electro-Optics*, OSA Technical Digest (Optical Society of America, Washington, DC, 2020), p. JW2B.9.
- [48] S. Steinke, J. H. Bin, J. Park, Q. Ji, K. Nakamura, A. J. Gonsalves, S. S. Bulanov, M. Thévenet, C. Toth, J.-L. Vay, C. B. Schroeder, C. G. R. Geddes, E. Esarey, T. Schenkel, and W. P. Leemans, Acceleration of high charge ion beams with achromatic divergence by petawatt laser pulses, *Phys. Rev. Accel. Beams* **23**, 021302 (2020).
- [49] K. V. Lezhnin and S. V. Bulanov, Laser ion acceleration from tailored solid targets with micron-scale channels, *Phys. Rev. Res.* **4**, 033248 (2022).
- [50] X.-L. Zhu, W.-Y. Liu, M. Chen, S.-M. Weng, P. McKenna, Z.-M. Sheng, and J. Zhang, Bunched Proton Acceleration from a Laser-Irradiated Cone Target, *Phys. Rev. Appl.* **18**, 044051 (2022).